Pattern formation during the growth of *Physarum*

João Bernardo Neves Blanchet Ferreira[1,*]

[1]*Department of Physics, Instituto Superior Técnico, Universidade de Lisboa, Av. Rovisco Pais 1, 1049-001 Lisboa, Portugal*

Physarum polycephalum is a fungi that displays highly adaptive vessel networks. Commonly known as the true acellular slime mould, it continuosly evolves its vein formation, optimising its food sharing capabilities as a result of reaction to simple stimuli, without rational control. Studying this organism may allow greater insight on angiogenic processes, such as cancer development, and on bioinspired algorithm for network solving, for instance transport networks. In this work, several growth and adaptation models are developed and tested, so as to construct a model that can fully replicate *Physarum*'s behaviour. Results show that the existing models are insuficcient and incompatible with *Physarum* growth. It is also shown that, under certain conditions, the developed adaptation model is able to construct minimum spanning trees and Steiner minimum trees for small numbers of vertices n. The latter is known to be an NP-complete problem.

Keywords: *Physarum polycephalum*, Diffusion, Adaptation, Minimum spanning tree, Steiner minimum tree

I. INTRODUCTION

Physarum polycephalum, despite being a nonneuronal organism, displays several high-level behaviours. Firstly, though without a brain, it is capable of an externalised spatial memory, a possible precursor to the internal memory of higher organisms [1]. This ability to store and retrieve information relative to past events provides the slime mould with decision-making skills. When comparing multiple options, based on the magnitude and frequency of the rewards, it is able not only to make correct and adaptive decisions but also irrational choices, much like a human being, which was often viewed as a byproduct of brain circuitry [2].

Being a single multinucleate cell, it behaves as a colony. Each nuclei contributes to a natural pulsating behaviour, and should attractive, and likewise repulsive, stimuli be detected, pulses increase in frequency, or decrease, respectively. Consequently, protoplasm can be shifted accordingly, which in turn allows structural proteins, such actin and myosin, to reach stimulus sites and form new vessels. This to-and-fro motion of flow, known as shuttle streaming, in itself a complex behaviour [3], allows not only expansion but also motion. Despite continuously developing new vessels, *Physarum* also optimises its vein network, so as to distribute all the food evenly among the entire cell. Although initially several thin veins exist, vessels that transport more flow in the complete network gradually become thicker, such that nutrients may be efficiently shunted, from one end to another. Amazingly, this venous structure shows a trade-off between fault-tolerance and total length, meaning minimal cost [4]. Additionally, its network sometimes displays the same topology as the Steiner minimal tree [5], known problem of graph theory.

Graph theory is responsible for the study of graphs, networks or structures that establish relations between vertices through edges, having a broad application scope, from communication and sensor networks — when considering network coverage or channel capacity —, to traffic and transportation — when connecting different cities with roads.

*Electronic address: jbblanchet@sapo.pt

Usually, in all application fields, rather than having a graph to begin with, it is necessary to construct it. The question that remains is, given a set of vertices and a set of conditions or restrictions, what is the best set of edges that can be considered? The Steiner problem tries to answer what edges form the graph with minimal length, if additional vertices are allowed. Computing Steiner minimal trees, for a general planar point set, has been shown to be an NP-complete problem [6].

A. Objectives and Outline

The purpose of this thesis work is to develop a model for the network formation of *Physarum polycephalum* and is structured according to three essential milestones, projected to be achieved. The first step is to create a growth model that fully mimics *Physarum*'s growth into a complete non-optimal network. Next, the adaptation model is considered, such that, from a developed network, evolves into the optimal case. Finally, the merger of both developed models is tested and matched with the *in vivo* behaviour of *Physarum*.

II. PHENOMENOLOGY OF *PHYSARUM POLYCEPHALUM*

A. Life cycle

Physarum polycephalum (*Pp*) is commonly known as a true acellular slime mould, displaying high adaptability to environmental changes as a result of its complex life cycle with both haploid and diploid phases. When conditions are appropriate, *Pp* exists as a thin, streaming and multinucleate mass that creeps along in an amoeboid fashion — a plasmodium.

In a low nutrient concentration environment, **Figure 1(a)**, the plasmodium grows towards the nutrient source by developing pseudopodium-like processes. If, however, it finds itself in a high nutrient concentration environment, it spreads radially, as in **Figure 1(b)**. During these growth phases, the plasmodium displays a pulsating behaviour of protoplasm, and exposure to stimuli modulates the frequency of these pulses — attractive stimuli

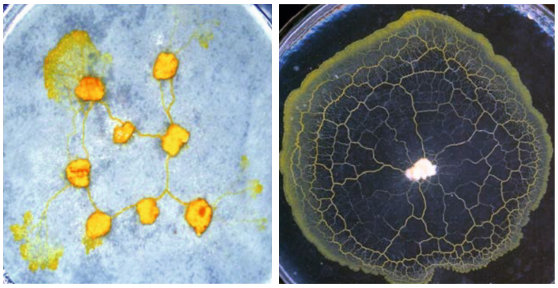

(a)Low concentration. (b)High concentration.

FIG. 1: *Pp* growth pattern. Source: [7].

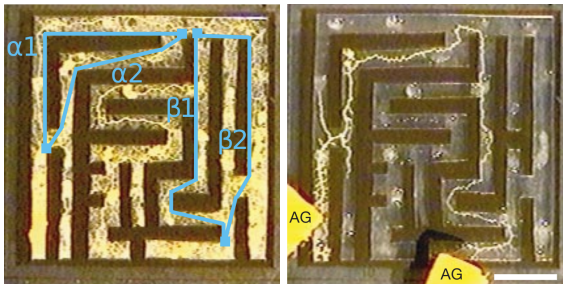

(a) (b)

FIG. 2: Maze solving by Pp. In (a), blue bold lines indicate possible paths, with $\alpha_2 < \alpha_1$ and $\beta_1 < \beta_2$. Scale bar of 1 cm. Source: [10].

increase the frequency, bulging outwards and thickening the affected vessels, while repulsive ones decrease it, retracting both membrane and vessels. As a result of this to-and-fro transport of protoplasm, called shuttle streaming, structural proteins such as actin and myosin are shifted towards stimulated regions, allowing not only motion but also growth. This growth front is fan-shaped, with thicker tubules at the base of the fan, spreading outwards and branching into thinner outer ends.

B. Optimisation capabilities

One very interesting aspect of this web of vessels is that, as time passes, it is progressively optimised, in the sense that the paths that connect the nuclei in the least distance get thicker, while the rest shrinks and eventually disappears. This vascular network is highly dynamic, with constant reassembly of its vessels as a response to changes in its environment. Be it a positive stimuli, such as a new food source, or a negative one, such as increase in luminosity, the plasmodium reorganises and again optimises its morphology, as to share the nutrients amongst all the nuclei in approximately minimum paths.

Despite being a simple life form, without any sort of voluntary control, *Pp* shows signs of high level optimisation, modulated by simple responses to environmental stimuli. Studies have shown that it is capable of an externalised spatial memory [1], a possible precursor of internal memory of higher organisms, and displays decision-making skills [2], both rational and irrational, much like human beings. Thus, it displays some sort of computational capability, with alternative logic gate and computer builds currently being studied [8, 9]. This proficiency has been put to use in solving certain practical optimisation problems, such as maze solving [10] and network optimisation [4], shown in **Figures 2** and **3** respectively.

III. GROWTH MODELS

A. Diffusion

The first test that may be conceived is to consider growth where nutrient is readily available for the organism to use and grow. Diffusion is the simplest mechanism to share these nutrients inside the organism. In a diffusive process, there is a net movement of molecules from a region of high concentration to a region of low concentration, *i.e.*, the movement of a substance down a concentration gradient. Intuitively, a diffusing substance spreads out, moving away from the area of high concentration. One visual example is the diffusion of a red dye droplet in a glass of water. At first, the droplet is concentrated with a bright red colour, but as diffusion occurs, it becomes smeared and the whole glass becomes slightly tinted. The diffusive process results in mixing, where molecules are dispersed in the volume. This is not be confused with other processes, such as advection, where there is bulk transport, *i.e.*, molecules behave as a static package that goes with the flow. Mathematically, this corresponds to

$$\frac{\partial \varphi}{\partial t} = D\ \nabla^2 \varphi, \tag{1}$$

with φ the concentration of food and D the diffusivity of the medium. Assuming a 2D behaviour, a discrete grid will register food concentration $\varphi_{i,j}$, and another the state of the cell $s_{i,j}$, such that an empty cell may be distinguishable from a *Pp* cell and a food source, respectively, states `0`, `1` and `2`. Considering finite differences, the previous equation becomes

$$\varphi_{i,j}^{t+1} = D\ \frac{\Delta t}{(\Delta x)^2}\ \left(\varphi_{i+1,j}^t + \varphi_{i-1,j}^t + \varphi_{i,j+1}^t + \varphi_{i,j-1}^t - 4\varphi_{i,j}^t \right). \tag{2}$$

However, this does not take into account the diagonal neighbours, nor does it represent a bounded diffusion, since there is no restriction regarding the cell state. Considering the results of **Dilão and Sainhas** [11], this can be further corrected to

$$\begin{aligned} \varphi_{i,j}^{t+1} = \varphi_{i,j}^t + \frac{1}{9}\ \Big[& f(s_{i,j}^t,\, s_{i+1,j}^t)\ \ (\varphi_{i+1,j}^t - \varphi_{i,j}^t) \\ & +\ f(s_{i,j}^t,\, s_{i-1,j}^t)\ \ (\varphi_{i-1,j}^t - \varphi_{i,j}^t) \\ & +\ f(s_{i,j}^t,\, s_{i,j+1}^t)\ \ (\varphi_{i,j+1}^t - \varphi_{i,j}^t) \\ & +\ f(s_{i,j}^t,\, s_{i,j-1}^t)\ \ (\varphi_{i,j-1}^t - \varphi_{i,j}^t)\ \Big] \\ & + \frac{1}{36}\ \Big[f(s_{i,j}^t,\, s_{i+1,j+1}^t)\ \ (\varphi_{i+1,j+1}^t - \varphi_{i,j}^t) \\ & +\ f(s_{i,j}^t,\, s_{i+1,j-1}^t)\ \ (\varphi_{i+1,j-1}^t - \varphi_{i,j}^t) \\ & +\ f(s_{i,j}^t,\, s_{i-1,j+1}^t)\ \ (\varphi_{i-1,j+1}^t - \varphi_{i,j}^t) \\ & +\ f(s_{i,j}^t,\, s_{i-1,j-1}^t)\ \ (\varphi_{i-1,j-1}^t - \varphi_{i,j}^t)\ \Big], \end{aligned} \tag{3}$$

where

$$f(s_{i,j},\, s_{k,l}) = \begin{cases} 1 & \text{if } s_{i,j} \neq 0\ \wedge\ s_{k,l} \neq 0, \\ 0 & \text{if } s_{i,j} = 0\ \vee\ s_{k,l} = 0. \end{cases} \tag{4}$$

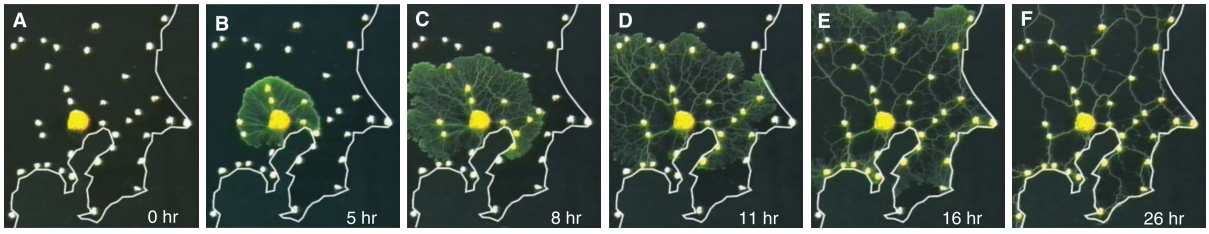

(a) (b) (c) (d) (e) (f)

FIG. 3: Network solving by Pp, for the japanese rail network case. Each food source matches a major city, with the inoculation site representing Tokyo. Source: [4].

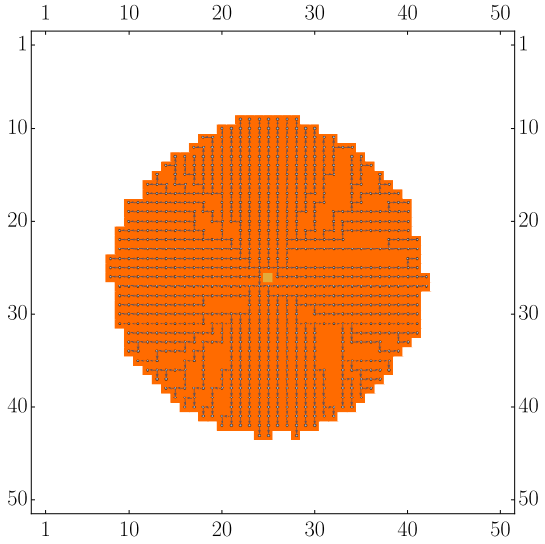

FIG. 4: Result of diffusive growth overlaid with growth graph structure after 5000 iterations.

The additional calibration equation $D\Delta t/(\Delta x)^2 = 1/6$ is also considered. With these considerations, diffusion is well defined. As such, to implement growth, a threshold value of food c_T is defined, such that, if a cell has food $c_{i,j} > c_T$, it occupies a randomly chosen vacant adjacent cell. Assuming that growth represents the creation of new vessels, the sequence of growth, from father to daughter cells, is recorded on a graph, **Figure 4**. Even though only the veins that connect the starter cell with the perimeter are highlighted, one can see that almost every growth sequence in the up, down, left and right directions can be traced back almost directly to the starter site. Additionally, any bifurcation occurs either near the starter site or in the diagonal directions. This is a result of the different speed for different directions, a result of the $1/4$ and $1/36$ factors of **Equation 3**, and due to cells only being allowed to grow in the up, down, left and right directions. Results of the diffusive growth are not compatible with *Pp* behaviour.

B. Eden model

Eden [12] developed a mathematical model in order to answer the following question: starting from a single cell which may divide, and its daughter cells may also divide again and again, what are the structural properties of the resulting colony of cells and how do various possible constraints effect the architecture? In order to simplify the growth process, cells only have growth capabilities. At each time step, one adjacent vacant is randomly selected, with equal probability, to become occupied. Iterating this behaviour nets **Figures 5(a)** and **5(b)**. Both display the same structure, qualitatively, and when analysing the degree of the underlying graph, and average value of ~ 3 is obtained. This result is in agreement with [13], suggesting this may be the correct approach.

The next step would be to consider manipulating the probability of each cell. **Mansfield and Klushin** [14], in the context of polymer crystallisation, proposed a generalisation of the Eden growth model, suggesting that each cell has a probability dependent on the number of neighbouring cells. It is assumed that having i neighbours contributes a ratio f_i, which is then normalised to give the probability. Modifying these parameters allows control over the overall aspect of the growth front. When $f_1 = f_2 = f_3 = f_4 = 1$, the standard Eden model is obtained. In **Figure 5(c)**, the growth pattern for $f_1 = 1$, $f_2 = 2$, $f_3 = 3$, $f_4 = 4$ is shown, displaying a similar result but with fewer holes.

Moreover, how can the probability of each cell carry any meaning? It can be assumed that the farther a cell is from the source, the longer food will take to reach it. This, in turn, means that, over time, less food will reach the cell, meaning less nutrients will be available for growth. The inverse of the total length of each path, from food source to each perimeter, is thus considered to control growth. To take into account the number of neighbours each empty cell has, the ratio will be equal to the sum of each individual path's factor. This additional consideration will even the growth probability between cells that are connected by shorter paths and cells that are irrigated by multiple longer paths. Results of these considerations are shown in **Figure 5(d)**.

C. Hagen-Poiseuille flow

With the results of the previous section, food is effectively reintroduced in the model. In order to calculate food flow, the Hagen-Poiseuille equation is considered. This determines the pressure drop of a laminar flow of incompressible Newtonian fluid, with null acceleration, through a cylindrical canal, with a constant cross section that is substantially smaller than its length. With these considerations, the velocity of the flow is given by

$$\mathbf{u} \equiv u_z(r) = -\frac{R^2 - r^2}{4\mu}\frac{\Delta p}{L}, \tag{5}$$

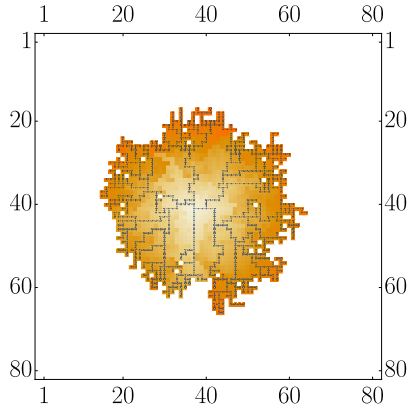

(a)Standard Eden model
($t = 1500$ iterations)

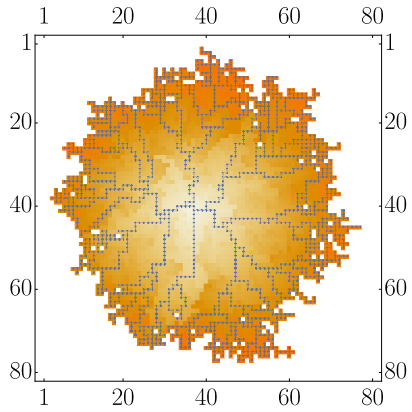

(b)Standard Eden model
($t = 3500$ iterations)

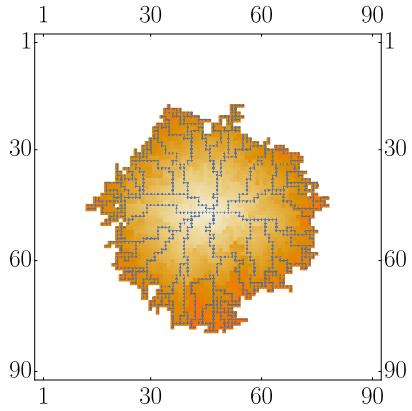

(c)Generalised Eden model with
$f_1 = 1$, $f_2 = 2$, $f_3 = 3$, $f_4 = 4$
($t = 2500$ iterations)

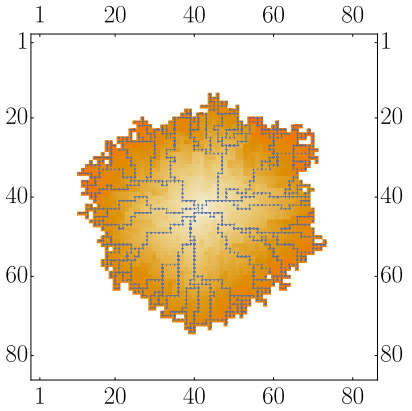

(d)Length-based Eden model
($t = 2500$ iterations)

FIG. 5: Comparison of three studied Eden models.

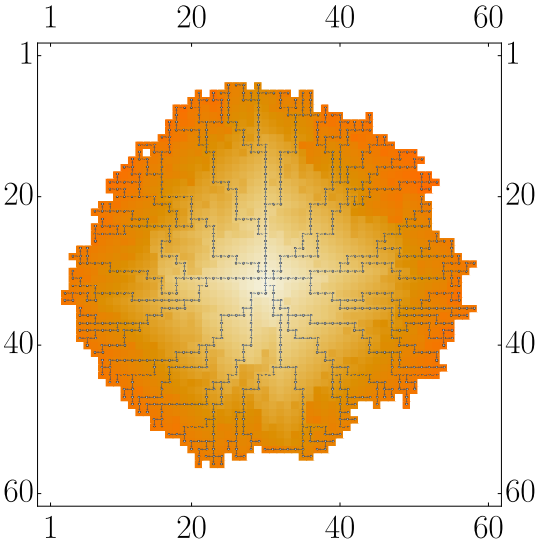

FIG. 6: Growth pattern obtained using Hagen-Poiseuille flow as the probability.

with R and L the radius and length of the canal, μ the viscosity of the fluid and Δp the difference in pressure between both ends. Integrating over the cross section, gives the flow

$$Q = -\frac{\pi R^4}{8\mu}\frac{\Delta p}{L} = -\frac{D}{L}\Delta p, \tag{6}$$

with D a simplified diffusivity of the medium. The sum of all flows that reach a given vertex $\sum_j Q_{i,j} = Q_i$ will state whether there is inflow, outflow or, conservation. If Q_i is negative, then i is a food source, if it is positive, a sink, and if null, a passage node, allowing the placement of food sources and sinks. Each vertex will contribute with one equation. Thus a linear system, that takes into account the properties of each edge, is defined. This linear system is then solved for the pressure of each node, by **Equation 6**.

Naturally, the food source will remain the central initial site, however, so that every sink remains on the outside of the cell, as the previous cases, temporary links will be created and added to the graph to calculate the flow each cell intakes. This again nets a similar structure as all the previous cases, retaining bifurcations with degree ~ 3, **Figure 6**. However, these growth models do not fully mimic *Pp*'s behaviour, as only bifurcations emerge but junctions from different paths do not occur. For this to happen, it is assumed that adaptation may play a role in selecting which paths remain.

IV. ADAPTATION MODELS

A. Simple cases

Having developed flow dependent growth models, flow-based adaptation models are tested, such that both can be compatible with each other. Despite the more common model by **Tero *et al.*** [4], **Miyaji and Ohnishi** [15] have proved that

$$\frac{\mathrm{d}D_{ij}}{\mathrm{d}t} = |Q_{ij}| - D_{ij} \tag{7}$$

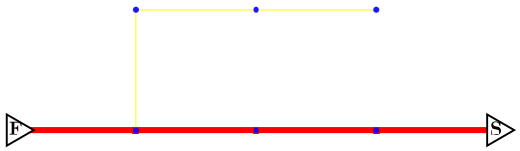

FIG. 7: Final configuration with dead end after 5000 iterations with $\Delta t = 10^{-3}$. Thickness proportional to $D_{i,j}$.

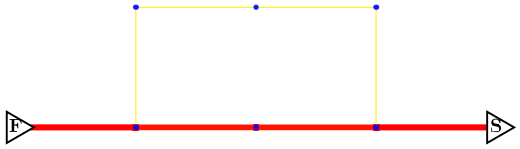

FIG. 8: Final configuration with alternative path after 5000 iterations with $\Delta t = 10^{-3}$. Thickness proportional to $D_{i,j}$.

is sufficient for creating minimal paths between two points. This is then discretised, which gives

$$D_{ij}^{t+1} = D_{ij}^{t} + \Delta t \ \left(\ \left|Q_{ij}^{t}\right| - \alpha D_{ij}^{t} \ \right), \tag{8}$$

with α a parameter to moderate how intense the shrinking behaviour should be. Intuitively, this represents the strain or risk Pp is exposed to, with higher or lower values of α corresponding to harder or better overall conditions, respectively. For simplicity, it is assumed to be constant, $\alpha = 1$.

Firstly, simple cases where there is only one path are studied, followed by graphs with multible possible solutions, *i.e.*, more than one path has minimal length, and finally the maze structure, as seen in [4], is replicated, respectively in **Figures 7**, **8**, **9** and **10**. In **Figures 7** and **8** only the minimal path persists. When two paths of equal length exist, both remain but with have smaller diameter, as flow is split equally between them, **Figure 9**. As can be seen in **Figure 10**, the maze is a combination of simpler graphs, with dead ends and alternative ineffective paths, and the previous algorithm is able to conclude the minimal path, when there is no ambiguity. It is important to note that it does not match the results in **Figure 2** since the simulated maze is an approximation of the maze itself, with perfectly orthogonal edges, while Pp has slight differences in length.

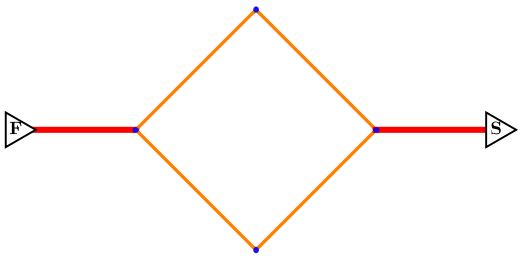

FIG. 9: Final configuration with bifurcation and redundant paths after 5000 iterations with $\Delta t = 10^{-3}$. Thickness proportional to $D_{i,j}$.

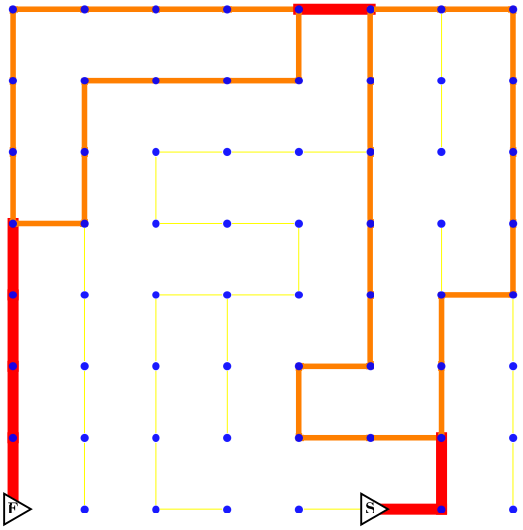

FIG. 10: Final configuration for the adapted network for the maze from [4] after 5000 iterations with $\Delta t = 10^{-3}$. Thickness proportional to $D_{i,j}$.

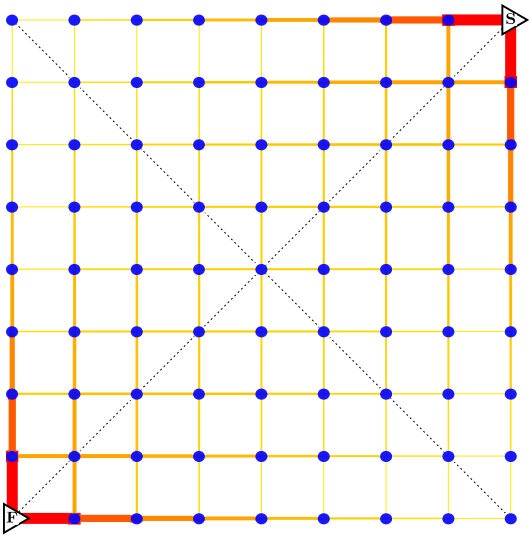

FIG. 11: Final configuration for a $\mathbf{9} \times \mathbf{9}$ grid after 5000 iterations with $\Delta t = 10^{-3}$. Thickness proportional to $D_{i,j}$.

B. Degenerate cases

Additionally, a grid graph, where every path has the same total length, is also studied. Contrary to intuition, even if all paths have the same total length, when adaptation acts over the grid, not all links share the same thickness, **Figure 11**. It is possible to remark, however, that links closer to the imaginary diagonal linking the food source and sink are thicker than those farther. Despite this variability, every grid displays both diagonal and anti-diagonal symmetry. This emerging symmetry can be explained by remembering that the linear system is solved considering conservation of flow in every node rather than equidistribution of flow for every edge.

However, distorting the grid, forcing different lengths for different edges between each node, will again net the expected trivial case where there is only one path with minimal total length, **Figure 12**.

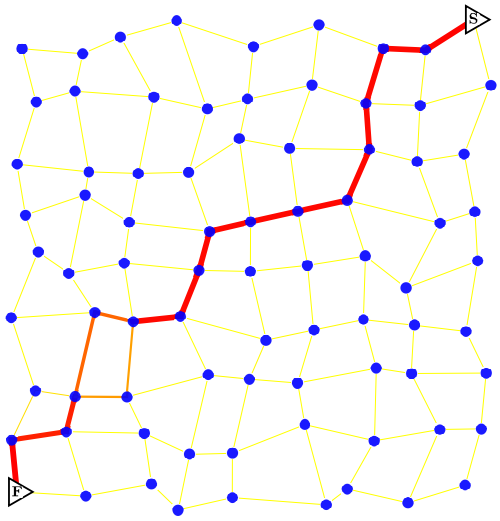

FIG. 12: Final configuration for a distorted $\mathbf{9} \times \mathbf{9}$ grid after 50000 iterations with $\Delta t = 10^{-3}$. Thickness proportional to $D_{i,j}$.

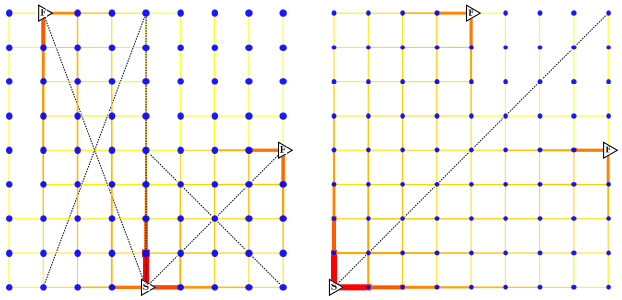

(a) (b)

FIG. 13: Final configuration for a $\mathbf{9} \times \mathbf{9}$ grid with 3 non-zero nodes after 15000 iterations with $\Delta t = 10^{-3}$. Symmetries shown in dashed lines. Thickness proportional to $D_{i,j}$.

In real-life, when confronted with several food sources, *Pp* adapts accordingly. Thus, the adaptation mechanism is tested again, now with an additional sink, to check whether any common path arises, **Figure 13**. However, adding another sink forms two independent subgraphs. Each subgraph corresponds to an individual grid graph and, despite edges common to both subgraphs being slightly thicker, as a result of constructive interference, no common minimal path is strengthened.

Results relative to grid graphs show that this grid structure cannot be used as the underlying structure for growth, as it would introduce an unsolvable ambiguity. To avoid this square lattice structure, the next step is to study random graphs.

C. Delaunay triangulation

In order to test if these results are a consequence of the underlying square lattice, a Delaunay triangulation is considered. Given a point set $\mathbf{P}$ in a plane, a Delaunay triangulation $DT(\mathbf{P})$ is a triangulation made such that no point in $\mathbf{P}$ is inside the circumcircle of any triangle in $DT(\mathbf{P})$.

Despite this change, when considering two food sources and one sink, the result is not altered, as two paths still exist independently, **Figure 14(a)**. However, as there no longer is a structure with degenerate paths, the solution resembles a minimum spanning tree. For larger number of vertices, with certain placement of food sources and sinks, more minimum spanning trees are obtained, **Figures 14(b)** and **14(c)**, with the former being cyclic.

Tero *et al.* [4], at each time step, randomly selected two vertices as food source and sink. However, for the adaptation model to match *Pp* behaviour, nodes acting as food sources and sink must remain fixed. Nonetheless, it may be interesting to allow their behaviour to swap at each time step. Having defined a fixed set of vertices to act as either food source or sink, at each time step, one node of the fixed set is chosen to act as a food source, while the rest are sinks. Results show approximate Steiner minimal trees, **Figure 15**.

However, for this particular setup to work, a noticeably large time step Δt is required. This effectively induces an aggressive bang-bang control on the system, i.e., vessels have no inertia when reacting to changes in flow and instantaneously adapt. Together with the random node behaviour swapping, these two problems give rise to halting problems, meaning there is no clear criteria to know when to stop.

D. Volume conservation

Results obtained using flow-based models have shown that this method may have some sort of systematic error that **Tero *et al.*** [4] and **Nakagaki *et al.*** [10] are not aware of. In Hagen-Poiseuille flow, the fluid is assumed to be incompressible. Thus, flow-based models must conserve the total volume of the network throughout the simulation. **Alim *et al.*** [16, 17], while studying the contractile behaviour of *Pp*, shows that the amount of fluid within a network is fixed and that, for a region to expand, a contraction follows elsewhere.

To determine the total volume of the network, the cross section is integrated in every path, *i.e.*,

$$V = \int_{\Omega} \pi r^2(s)\ \mathrm{d}s. \tag{9}$$

However, since $D_{i,j} = {}^{\pi r_{i,j}^4}/_{8\eta} \propto r_{i,j}^4$, this equation can be approximated to

$$V \propto \sum_{i \neq j} \sqrt{D_{i,j}}\ L_{i,j}. \tag{10}$$

Registering V at each time step produces **Figure 16**. This shows that volume is not conserved throughout the simulation and that the Hagen-Poiseuille flow cannot be correctly applied in this situation. As a result of **Equation 8**, the volume converges to a value that is proportional to the total number of edges belonging to the minimal path solution.

Contrary to what is expected, from the results of [4, 10], although flow-based models may adequately solve simpler forms of graph network problems, it is therefore shown that they do not strictly replicate, in any way whatsoever, *Pp*'s natural behaviour, regardless of having fixed or random behaviour, for a given vertex set.

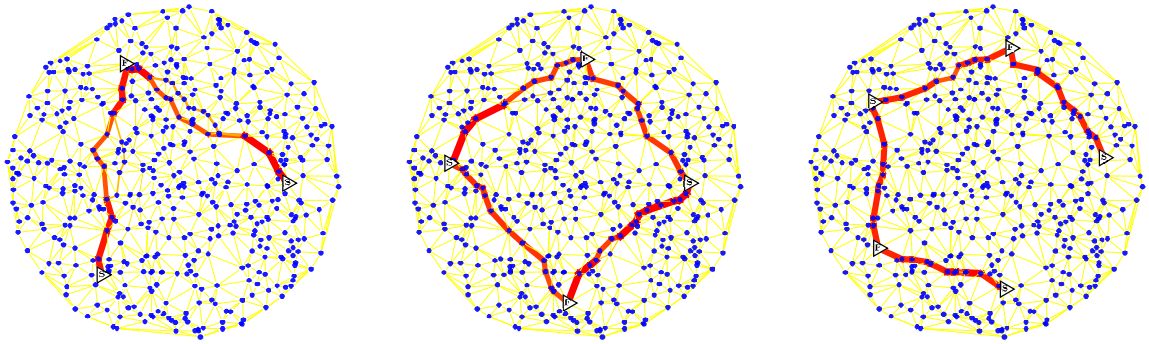

(a)One food source and two sinks. (b)Two food sources and two sinks. (c)Two food sources and three sinks.

FIG. 14: Final configuration for a Delaunay triangulation of a random point set after 5000 iterations with $\Delta t = 10^{-1}$. Note the approximately minimal spanning trees.

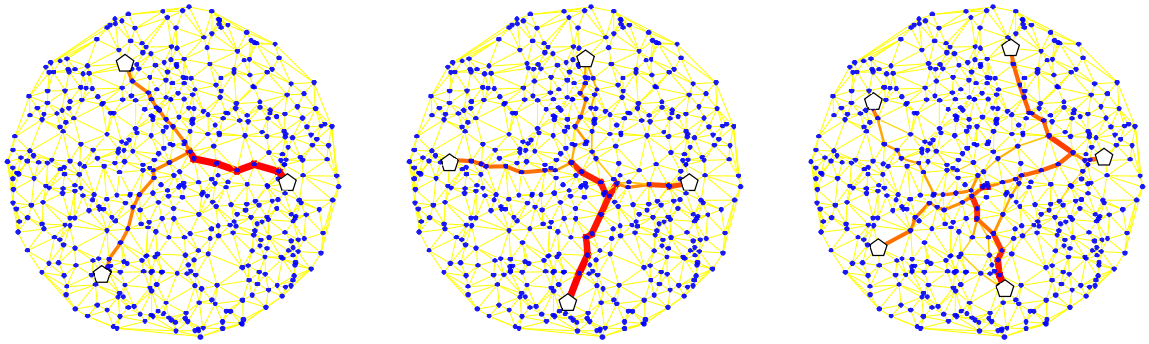

(a)Three vertices. (b)Four vertices. (c)Five vertices.

FIG. 15: Final configuration for a Delaunay triangulation of a random point set, with nodes with random behaviour, after 100 iterations with $\Delta t = 1$. Note the approximate Steiner minimal trees.

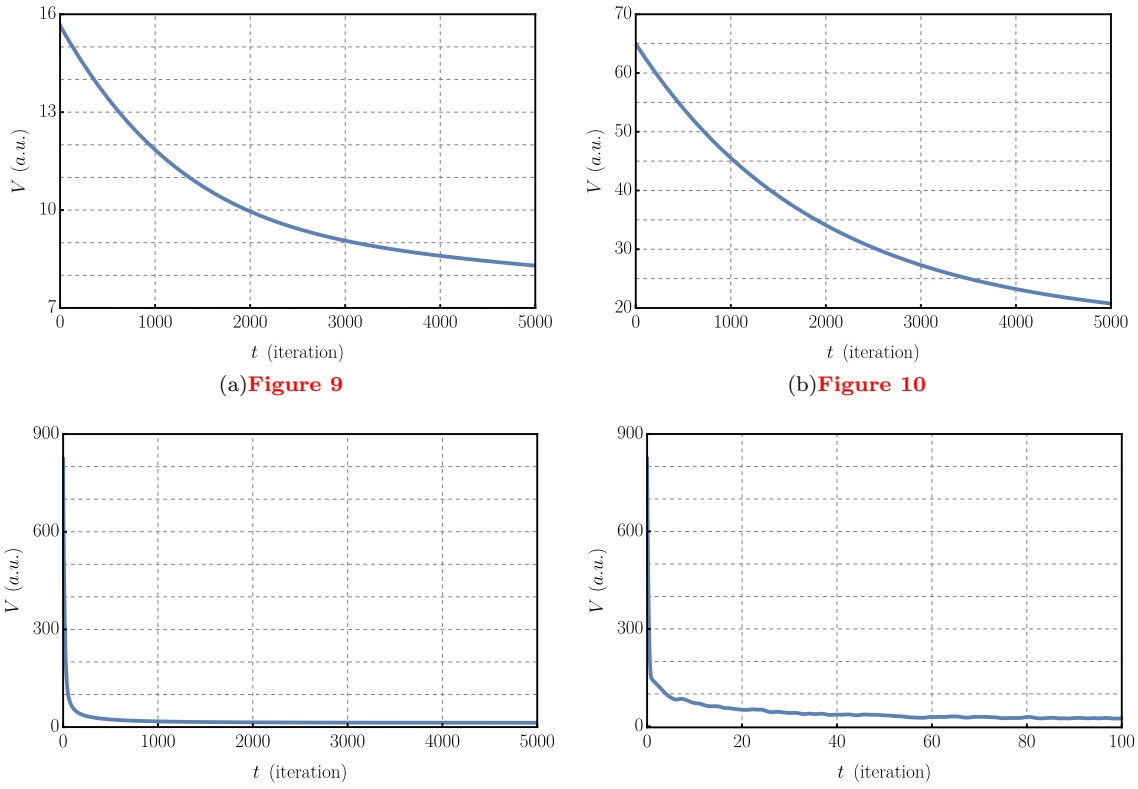

(a)**Figure 9** (b)**Figure 10**

(c)**Subfigure 14(a)** (d)**Subfigure 15(a)**

FIG. 16: Evolution of the total volume of a selection of the previously studied graphs. Volume is not conserved throughout the simulations, showing that the Hagen-Poiseuille flow can no longer be applied as the fluid is compressible.

V. CONCLUSIONS

In this work, the vessel network development of *Physarum polycephalum* was studied and several attempts to model its growth were made. Fully modelling *Physarum polycephalum* still persists as an hard, and exciting, challenge. Despite interest from a wide field of research, its complex behaviour, emergent from brainless responses to simple stimuli, remains only partly understood.

Firstly, its growth model was tested. Diffusion was first used as the process to moderate its growth, but, when analysing the cell growth sequence, it could not be compatible with the naturally occurring vein formation. The Eden stochastic model [12] was considered, being a model that does not rely explicitly on food. Interestingly, the result of the network having nodes of degree ~ 3 [13] emerged from this simpler model. This model was used as a stepping stone, being continuously refined by first adding a dependence on the number of neighbours, then considering that each neighbour was different and dependent on the total length its branch had, and, finally, converting this length to actual food flow, by implementing the Hagen-Poiseuille flow. Each modification allowed the model to retain its overall aspect, particularly the ~ 3 degree result, while progressively becoming a more real and natural growth model.

However, observing *Pp*'s natural behaviour, it is easily noted that vessels not only bifurcate during growth but also join and merge paths from different sources. Intuitively, from a graph topology point of view, these display the same structure. Thus, a growth model, with direct influence from intake of food sources, has been developed. This growth model may fully replicate other simpler life forms, other than *Physarum polycephalum*. Additionally, results from this model may present novel ideas for angiogenic processes, *i.e.*, vessel formation, which in turn may help in developing solutions to vascular disease, cancer, and neurodegeneration.

Lastly, with a possible growth model, its adaptation mechanism was studied. Since the developed growth model depended on nutrient flow, flow-based adaptation was considered, such that both of these could be compatible. Tests were made by gradually increasing the complexity of the network, from simple one path structure, to two path graphs, then the known maze structure, and finally grid networks. These step-by-step modifications were carried out in order to evaluate the efficiency of the mechanism regarding degenerate paths. Tests were extended to uneven number of food sources and sinks and to random graphs. Additionally, volume conservation of the graph structure was also studied.

However, all adaptation models depend on the existence of sinks, resultant of conservation of mass in the implementation of models. This assumption is biologically unrealistic. As a result, two food sources placed near each other repel growth in the area between them, rather than strengthen it, as observed in *Physarum* organisms. Moreover, simulation results show that volume is not conserved during simulations. This is not compatible with the initial assumptions of **Tero *et al.*** [4] and **Nakagaki *et al.*** [10], as Hagen-Poiseuille flow is, in fact, not applicable. It is also shown that the simpler model by **Miyaji and Ohnishi** [15] proves sufficient for shortest path calculations in graph structures.

[1] C. R. Reid, T. Latty, A. Dussutour, and M. Beekman, Proceedings of the National Academy of Sciences **109**, 17490 (2012).

[2] T. Latty and M. Beekman, Proceedings of the Royal Society B: Biological Sciences **278**, 307 (2010).

[3] S. J. Coggin and J. L. Pazun, Protoplasma **194**, 243 (1996).

[4] A. Tero, S. Takagi, T. Saigusa, K. Ito, D. P. Bebber, M. D. Fricker, K. Yumiki, R. Kobayashi, and T. Nakagaki, Science **327**, 439 (2010).

[5] A. Tero, T. Nakagaki, K. Toyabe, K. Yumiki, and R. Kobayashi, International Journal of Unconventional Computing **6**, 109 (2010).

[6] M. R. Garey, R. L. Graham, and D. S. Johnson, SIAM Journal on Applied Mathematics **32** (1977).

[7] J. Jones, *From Pattern Formation to Material Computation*, Emergence, Complexity and Computation, Vol. 15 (Springer, 2015).

[8] A. Schumann, International Journal of Parallel, Emergent and Distributed Systems **32**, 218 (2015).

[9] A. Adamatzky, *Physarum Machines: Computers from Slime Mould*, edited by L. O. Chua, A, Vol. 74 (World Scientific Publishing Company, 2010).

[10] T. Nakagaki, H. Yamada, and A. Tóth, Nature **407**, 470 (2000).

[11] R. Dilão and J. Sainhas, International Journal of Bifurcation and Chaos **8**, 1163 (1998).

[12] M. Eden, in *Proceedings of the Fourth Berkeley Symposium on Mathematical Statistics and Probability*, Vol. 4: Contributions to Biology and Problems of Medicine, edited by J. Neyman (University of California Press, Berkeley, California, 1961) pp. 223–239.

[13] W. Baumgarten, T. Ueda, and M. J. B. Hauser, Physical Review E **82**, 046113 (2010).

[14] M. L. Mansfield and L. I. Klushin, Polymer **35**, 2937 (1994).

[15] T. Miyaji and I. Ohnishi, International Journal of Pure and Applied Mathematics **47**, 353 (2008).

[16] K. Alim, G. Amselem, F. Peaudecerf, M. P. Brenner, and A. Pringle, Proceedings of the National Academy of Sciences **110**, 13306 (2013).

[17] K. Alim, N. Andrew, A. Pringle, and M. P. Brenner, Proceedings of the National Academy of Sciences , 201618114 (2017).